NANO LETTERS

2009
Vol. 9, No. 7
2654-2660

Electronic Structure of Few-Layer Epitaxial Graphene on Ru(0001)

P. Sutter,* M. S. Hybertsen, J. T. Sadowski, and E. Sutter

Center for Functional Nanomaterials, Brookhaven National Laboratory, Upton, New York 11973

Received April 1, 2009; Revised Manuscript Received May 8, 2009

ABSTRACT

The electronic structure of epitaxial monolayer, bilayer, and trilayer graphene on Ru(0001) was determined by selected-area angle-resolved photoelectron spectroscopy (micro-ARPES). Micro-ARPES band maps provide evidence for a strong electronic coupling between monolayer graphene and the adjacent metal, which causes the complete disruption of the graphene π-bands near the Fermi energy. However, the perturbation by the metal decreases rapidly with the addition of further graphene sheets, and already an epitaxial graphene bilayer on Ru recovers the characteristic Dirac cones of isolated monolayer graphene. A graphene trilayer on Ru behaves like free-standing bilayer graphene. Density-functional theory based calculations show that this decoupling is due to the efficient passivation of metal d-states by the interfacial graphene layer.

Graphene, an atomically thin sheet of sp^2 bonded carbon,[1] has shown fascinating materials properties and holds the promise for future carbon-based device architectures, owing to characteristics such as a very high carrier mobility[2] and long ballistic mean free path at room temperature,[3] and the possibility of opening a variable bandgap by confinement in nanoscale ribbons.[4] The interaction of graphene with metals may hold the key to realizing much of this potential. Epitaxy on transition metal substrates has recently been demonstrated as a rational synthesis route for producing macroscopic single-crystalline graphene domains.[5] If the growth is performed on metal foils or thin films, such metal-catalyzed graphene sheets can be isolated by etching away the substrate.[6,7] For the inverse situation, metal electrodes evaporated onto the surface of graphene, calculations[8] and first experiments[9] have shown metal-induced changes to the electrostatic potential in the graphene layer, which can give rise to a net electron- or hole-doping. While charge transfer doping is predicted for metals that interact weakly with graphene (e.g., Al, Cu, Ir, Pt),[8,10] for many transition metals (e.g., Rh, Ni, Co, Ru, and Pd), the interaction with graphene is so strong that its effects go beyond electrostatic band shifts,[8,11,12] causing the complete disruption of the characteristic Dirac cones via electronic coupling of graphene π-states with metal d-states near the Fermi energy. The linear π-band dispersion can be restored even for these strongly interacting metals, e.g., by alkali metal[12] or noble metal[13] intercalation, as demonstrated for graphene on Ni(111). An elegant alternative would be to employ the screening in graphene itself to achieve such a decoupling. In a few-layer graphene stack, the outermost layers could be screened from the metal d-states by the interfacial graphene sheets and would thus recover massless Dirac fermions, required for applications such as spin filtering.[14]

Experiments and calculations on graphene-metal interactions have focused primarily on monolayer graphene so far.[10,11,15] Our recent demonstration of layer-by-layer growth of macroscopic graphene domains on Ru,[5] however, enables the investigation of the effects of a nearby metal on the electronic structure of few-layer graphene over a wider thickness range. Here we explore these effects by in situ measurements of the band structure of large graphene domains with precisely tunable thickness on Ru(0001). We combine these measurements with ab initio calculations to provide a quantitative picture of the interaction of graphene with Ru(0001), representative of the broader class of transition metals that interact strongly with graphene.

Graphene epitaxy was performed on a Ru(0001) single crystal, as described in detail elsewhere.[5] Briefly, clean Ru(0001) is enriched with interstitial C by hydrocarbon (ethylene) exposure at temperatures above 1000 °C. A slow lowering of the sample temperature reduces the C solubility in the metal and causes C surface segregation, which in turn drives layer-by-layer graphene growth. We observed this process in real time by low-energy electron microscopy (LEEM). Graphene grows initially via formation of monolayer thick islands that rapidly expand to a size corresponding to the spacing of the initial nuclei (>200 μm) and coalesce to a complete graphene layer covering the entire Ru(0001) substrate. Upon completion of the monolayer, subsequent graphene layers nucleate and grow layer-by-layer, again

* To whom correspondence should be addressed. E-mail psutter@bnl.gov.

10.1021/nl901040v CCC: $40.75
Published on Web 06/08/2009

reaching macroscopic domain sizes. Here, we employed this growth to produce samples with well-defined thickness of one to three graphene layers.

Band structure [$E(k_x,k_y)$] maps were obtained at room temperature in situ in the LEEM instrument by collecting angle-resolved photoelectron spectra from micrometer-sized sample areas with a uniform number of graphene sheets (micro-ARPES). Synchrotron ultraviolet radiation (National Synchrotron Light Source beamline U5UA; photon energy $h\nu = 42$ eV, providing high surface sensitivity and photon intensity) incident normal to the sample was used to excite photoelectrons, which were energy filtered by an imaging energy analyzer (energy resolution <0.3 eV), and whose angular distribution was mapped in reciprocal space using the electron optics and detector system of the LEEM. The raw data comprised photoelectron angular distributions beyond the first Brillouin zone (BZ) for energies from −25 eV to +2 eV relative to E_F in increments of 0.1 eV. Projections along high-symmetry directions in reciprocal space were used to generate band structure maps along those directions.

The physical and electronic structure of graphene mono-, bi-, and trilayers on Ru(0001) was further investigated theoretically, using density functional theory (DFT) as implemented in VASP.[16−19] In order to identify trends with layer thickness and interface bonding, commensurate structures with the graphitic layers strained to match the calculated Ru lattice parameter ($a = 2.68$ Å) were used, similar to recent studies for SiC substrates.[20,21] The electron interaction with the ion cores was represented by ultrasoft pseudopotentials[22,23] and the local density approximation (LDA) in the Ceperley−Alder form was used.[24,25] The plane wave basis set was truncated using a cutoff of 340 eV. The surface BZ was sampled by a 15 × 15 mesh including the zone center. During relaxation, the Methfessel−Paxton smearing scheme (0.1 eV) was used,[26] and the final self-consistent potential for the band structure was determined by the modified tetrahedron approach of Blöchl with the same broadening parameter.[27] The Ru(0001) surface was modeled using an 11 monolayer slab with the middle 3 layers fixed at bulk lattice positions. Structural refinements were performed with graphene layers on both sides to a maximum force criterion of 0.05 eV/Å. To eliminate residual interactions between the graphitic layers on the front and back of the Ru slab, band structure calculations were performed for a graphitic layer on one side of the slab and the opposite side in the relaxed clean Ru(0001) structure. The maximum forces met the same criterion, and the asymmetry in the self-consistent potential had minimal impact on the position of key graphene-dominated electronic energy bands (<0.06 eV). The graphene bands are presented based on the projection of each Bloch state on spheres centered on particular C atoms. The cutoff criterion used was 10% of the maximum value sampled over the energy range of the graphitic σ and π bands. This enables visualization of the graphitic states that couple with the Ru states. The use of strained graphitic layers affects the calculated band dispersions, so a direct quantitative comparison with the measured band dispersion has not been made.

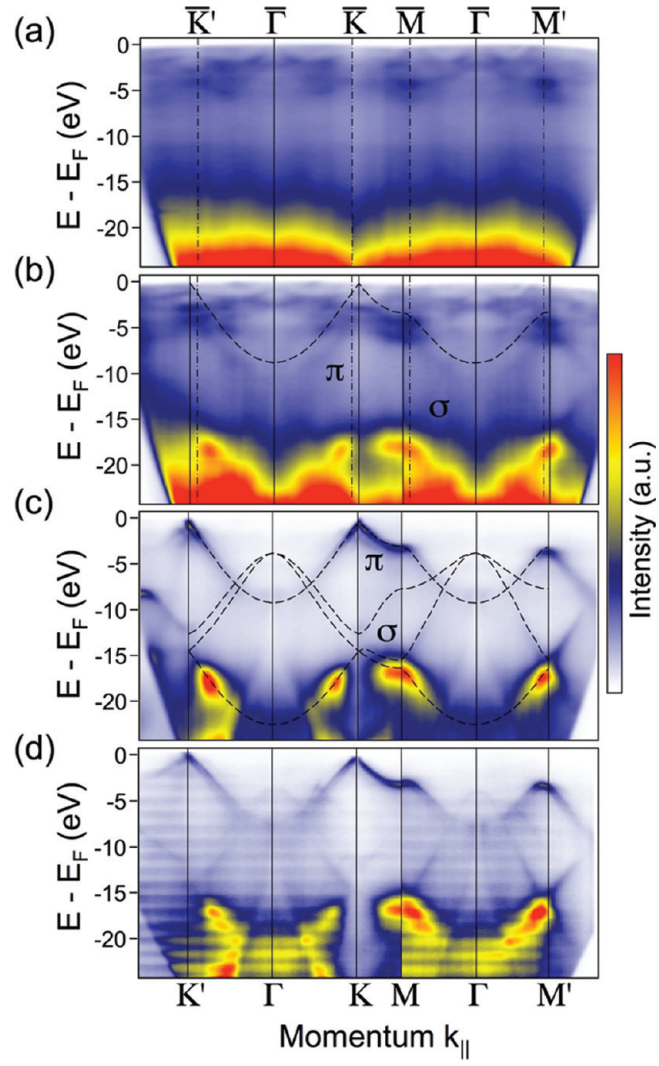

Figure 1. Micro-ARPES band structure maps of epitaxial monolayer, bilayer, and trilayer graphene on Ru(0001). (a) Ru(0001) substrate in an area that is not covered by graphene. (b) Monolayer graphene. Dashed line: π-band obtained from a tight-binding calculation for free-standing monolayer graphene.[29] (c) Bilayer graphene. Dashed lines: scaled DFT bands of free-standing graphene.[33] (d) Trilayer graphene; the periodic intensity modulation is due to slight variations in the incident photon intensity during the measurement.

Figure 1 shows the evolution of the electronic structure from the Ru(0001) substrate (Figure 1a) to epitaxial graphene on Ru(0001) with thickness of one (Figure 1b), two (Figure 1c), and three graphene layers (Figure 1d). Corresponding photoelectron energy distribution curves along the Γ−K direction are shown in Figure 2. The electronic structure of the Ru substrate, measured at low C coverage between monolayer graphene domains, is in good agreement with the calculated projected band structure of clean Ru(0001).[28] It shows the characteristic band gap between −3 and −6 eV near the zone center ($\bar{\Gamma}$), as well as two narrower gaps near $\bar{K}$. The growth of a single graphene layer on Ru(0001) has little effect on the occupied electronic bands within about 3 eV from the Fermi energy. At higher binding energy, well-

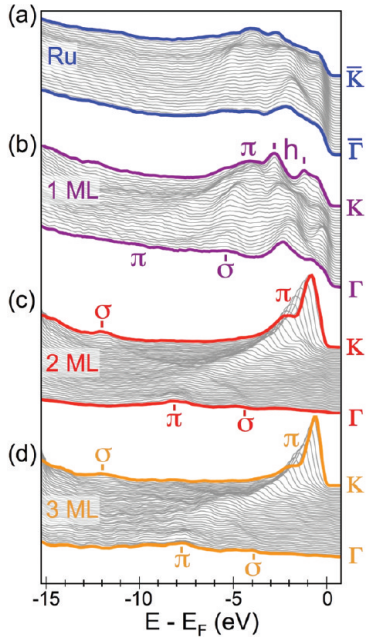

Figure 2. Micro-ARPES energy distribution curves (EDCs) of (a) bare Ru(0001), (b) epitaxial monolayer, (c) bilayer, and (d) trilayer graphene on Ru(0001). Thick lines mark Γ-point and K-point EDCs; thin lines illustrate the band dispersion along the Γ−K direction. Marked are σ and π-states, as well as metal-graphene hybrid (h) states in the case of the monolayer.

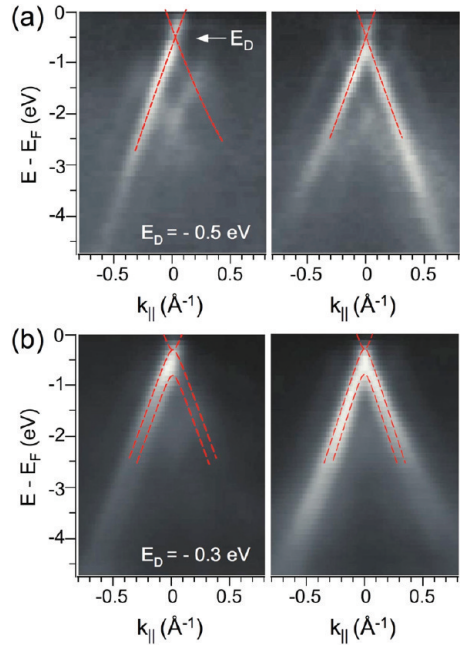

Figure 3. π-band dispersion near the K-point for bilayer and trilayer graphene on Ru(0001). (a) Micro-ARPES intensity maps near K for bilayer graphene/Ru(0001). Left: Projection along Γ−K. Right: perpendicular to Γ−K. (b) Micro-ARPES intensity maps near K for the trilayer. Left: Projection along Γ−K. Right: perpendicular to Γ−K. Dashed lines represent tight-binding bands, as described in the text.

developed π and weaker σ bands accompany the formation of the graphene monolayer. At high energies (>20 eV below E_F), finally the micro-ARPES spectra of both Ru(0001) and of the epitaxial graphene domains on Ru show a marked rise in intensity due to an increasing contribution of secondary electrons to the energy-filtered photoelectron signal. While this background is essentially featureless for Ru(0001), the formation of epitaxial graphene leads to a highly structured secondary electron angular distribution. A strongly anisotropic emission of secondary electrons is thus a telltale characteristic of the formation of sp^2-bonded graphene layers.

Compared with the π-band of isolated monolayer graphene, determined by a tight-binding calculation (ref 29 with $\varepsilon_{2p} = 0$) and shown as a dashed line in Figure 1b, the occupied π-band of the epitaxial graphene monolayer shows a uniform downward shift by about 2.6 eV throughout most of the BZ. Importantly, the π-band does not cross the Fermi level to give rise to the Dirac cones characteristic of free-standing monolayer graphene. These findings are consistent with a strong chemisorption of the graphene monolayer on the Ru substrate in agreement with conclusions reached in recent X-ray absorption[31] and angle-resolved photoemission[11] measurements. Similarly strong electronic coupling has been found for graphene on Ni(111)[13] and on several transition metal carbides.[32]

Continuing the graphene growth on Ru(0001) beyond the monolayer produces bilayer and finally trilayer domains sufficiently large (several micrometers) to selectively probe their electronic structure by micro-ARPES. The transition from an epitaxial graphene monolayer (Figures 1b and 2b) to a bilayer (Figures 1c and 2c) is accompanied by dramatic changes in the electronic structure. The most intense bands are now the occupied σ and π-bands. The π-band of the outer layer crosses E_F and shows a linear dispersion at K, i.e., recovers the signature of massless Dirac fermions characteristic of isolated monolayer graphene. For comparison, the energy bands of an isolated monolayer of graphene, based on a DFT calculation (stretched, following ref 33), are shown as an overlay in Figure 2c. There is an excellent overall match across the entire BZ if we assume an electron-doped epitaxial graphene layer whose Dirac point lies 0.5 eV below E_F. These measurements confirm the conclusion, drawn on the basis of the line shape of the double-resonant 2D Raman line,[5] that the outer sheet of bilayer epitaxial graphene/Ru(0001) has essentially the electronic structure of free-standing monolayer graphene.

Given that the outer sheet of the bilayer is essentially decoupled and has the characteristics of isolated monolayer graphene, the electronic structure of n-layer thick epitaxial graphene on Ru(0001) should, in general, correspond to that of $(n - 1)$-layer isolated graphene. A micro-ARPES map of the trilayer (Figure 1d) confirms this prediction. The expected π-band splitting due to the interlayer interaction (0.4 eV)[34] is clearly resolved along Γ−K (see also Figure 3b), and the additional screening modifies the electrostatic potential of the outer layers, causing measurable shifts of the bands.

Despite the fact that all graphene layers beyond the interfacial monolayer couple weakly to the metal substrate, the bilayer and trilayer both show residual doping due to charge transfer from the substrate. As in other systems, e.g., epitaxial graphene on SiC,[35,36] this doping progressively decreases with increasing thickness. The concomitant shift

of the Dirac energy away from E_F can be quantified by micro-ARPES intensity maps near the K-point of the BZ, as shown in Figure 3 along Γ−K, as well as perpendicular to Γ−K, that is, in a direction in which both branches of the π-band are symmetric.[37] The measured band dispersion is compared with the π-bands of isolated monolayer and bilayer graphene, calculated in the tight-binding approximation. The bilayer shows a linear π-band dispersion, which closely matches the tight-binding bands (ref 29 with $\varepsilon_{2p} = E_D = -0.5$ eV). The measured width of its bands is limited by the resolution of the energy analyzer. The bands of the trilayer appear much broader, and closely match the pair of parabolic bands computed for an isolated graphene bilayer using an approximate Hamiltonian[36] valid near K, with parameters $E_1 = E_2 = -0.30$ eV, and band velocity $v = 1.05 \times 10^6$ m/s. The Dirac energies, E_D, can be quantified by fitting the tight-binding bands to the micro-ARPES data. In this way, we deduce $E_D = -(0.50 \pm 0.05)$ eV for the bilayer, and $E_D = -(0.30 \pm 0.05)$ eV for the trilayer, respectively. Within the given energy resolution, the decoupled outer sheet of the bilayer preserves its semimetallic character, that is, no gap opening is observed around E_D,[37] suggesting that the symmetry of the A and B atom sublattices of the graphene sheet is not lifted by the underlying metal-graphene sandwich. The absence of sublattice symmetry breaking is confirmed independently by scanning tunneling microscopy (STM),[38] which images both sublattices equivalently as in graphene/SiO_2.[39] The Fermi velocity of $(1.0 \pm 0.1) \times 10^6$ m/s, deduced from the linear π-band dispersion of the bilayer is in excellent agreement with electron group velocities in exfoliated graphene.[1] Finally, Figure 3 shows fainter replicas of the intense π-bands for both bilayer and trilayer epitaxial graphene on Ru(0001). Similar replica bands observed for graphene on SiC(0001) were ascribed to final state diffraction by a $(6\sqrt{3} \times 6\sqrt{3})$ R30° reconstructed interfacial layer.[35] For few-layer graphene on Ru(0001), the moiré of the inner graphene layer creates a periodic interface structure, which could give rise to analogous diffraction effects. An alternative interpretation, the generation of an in-plane superlattice[10,40] in the top sheets of the bilayer and trilayer by a periodic potential due to the interfacial moiré, cannot be ruled out completely. DFT calculations (below) suggest a rather small variation of the electrostatic potential (<0.3 eV) in the top sheet of the bilayer and even smaller for the trilayer, which would give rise to gaps at the mini-BZ boundary too narrow to resolve in our experiment.

We further explored the origins of key features identified in our measurements, that is, the strong interfacial bonding of the graphene monolayer and the progressive decoupling with the addition of further graphene layers, via DFT calculations, using commensurate structures with the graphitic layers strained to the calculated Ru lattice constant. Because of the large mismatch (∼10%), the calculated strain energy is relatively large (1.06 eV per two C atoms), which provides the driving force for the formation of the moiré pattern observed experimentally.[41] Strain also shifts the calculated work function of isolated graphene from 4.5 to 5.2 eV. While the work function difference with respect to

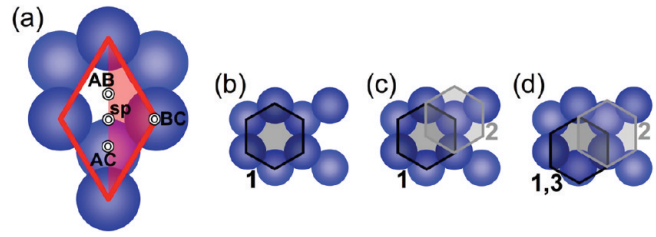

Figure 4. (a) Illustration of the portion of the surface unit cell (shaded part of rhombus) sampled by the centroid of graphene hexagons to form commensurate structures covering the interface registries occurring in the relaxed graphene/Ru moiré observed experimentally. Specific high-symmetry cases are labeled. Dark- and light-shaded circles indicate surface and subsurface Ru atoms, respectively. (b) Example of a commensurate monolayer graphene structure with *AB* interface registry. (c) Example of a commensurate bilayer graphene structure. The black hexagon indicates the first (inner) graphene layer with *AB* alignment to Ru, and the gray hexagon the second (outer) layer in Bernal stacking (*BC* registry). (c) Illustration of a commensurate trilayer graphene structure with split alignment of the inner graphene layer to Ru. The third (outermost) graphene layer is vertically aligned to the first (inner) layer.

Ru (calculated to be 5.4 eV) is one factor in the final electronic structure of the graphitic layers on Ru, the local chemical interactions turn out to be significant, as found for interfaces with other transition metals.[8]

To evaluate the interface bonding, we sampled the registry of the graphene layer to Ru(0001) as illustrated in Figure 4. Sites of C atoms directly above surface Ru, subsurface Ru, and hollow sites are designated *A*, *B*, and *C*, respectively.[8] The case where the C−C bond is centered on the surface Ru site is designated split. We sampled the interface registry by fixing the centroid of the graphene hexagon relative to the bulk portion of the Ru slab within half of the surface unit cell (Figure 4 a) for 10 symmetry-distinct cases that include the high symmetry registries shown in Figure 4b−d.

We first consider the binding of graphene to the Ru substrate, starting with a graphene monolayer. The binding energy for a prestrained graphene layer on Ru(0001) varies from 0.1 eV per two carbon atoms for the *BC* registry (layer spacing $\Delta Z_{Ru-C} = 2.20$ Å) to 0.9 eV for the split ($\Delta Z_{Ru-C} = 2.06$ Å) and *AC* ($\Delta Z_{Ru-C} = 2.12$ Å) cases. The binding energy for the *AB* registry is 0.8 eV ($\Delta Z_{Ru-C} = 2.12$ Å). All structures except the weakly bound *BC* registry show Ru−C bond lengths between 2.1 Å and 2.2 Å, close to the sum of conventional covalent radii. Together with the calculated binding energies, this proximity demonstrates a significant chemical interaction upon interface formation over most of the area of the experimentally observed moiré structure. The present LDA-based calculations suggest only small physical height variations (about 0.15 Å) across the moiré pattern.[42]

Introducing a second graphene layer with Bernal stacking has minimal impact on the interface structure and binding of the inner graphene layer to the Ru substrate for all registries considered. The spacing between the two graphene layers is large (3.42 to 3.52 Å) and matches that calculated for an isolated graphene bilayer expanded to the Ru(0001) lattice parameter (3.50 Å). The additional layer couples weakly to the interface system, and its binding energy (0.05

eV per two C atoms) is essentially the same as the interlayer energy of an isolated graphene bilayer. We probed the trilayer only for the *AB* and split cases, but come to similar conclusions.

We now turn to calculations of the electronic structure of the graphene layers on Ru(0001). The formation of a graphene monolayer on Ru(0001) significantly reduces the work function relative to the clean metal surface (5.4 eV). The actual value depends on the registry, spanning the range between 3.8 and 4.3 eV. The *AB* and split registries give the lowest and highest work function, respectively. The *BC* case with weak binding has a work function (4.2 eV) similar to the *AB* registry. The lowering of the work function is consistent with donor−acceptor type bonding between the graphene layer and the Ru surface. Charge is effectively transferred to the surface through electronic coupling of the π-bands with Ru d-states. Upon addition of a second graphene layer, the work function increases substantially to 4.7−5.0 eV. The trilayer shows a further increase by 0.2 eV. Overall, the computed work function changes reproduce the trends observed experimentally by photoelectron microscopy, which also show a sharp reduction of the work function from Ru metal to monolayer graphene on Ru, followed by progressive increases with the formation of bilayer and trilayer graphene.

An example of the energy bands for a graphene bilayer in *AB* registry on Ru(0001) is shown in Figure 5, in which projections on atom centered spheres are used to identify states characteristic of the inner and outer graphene layer. Considering the overall band structure, the interaction between the layers is weak. The band structure of the two layers is essentially decoupled, except near the **K**-point for energies near E_F, where interactions at band crossings are apparent. Comparing with an isolated, strained graphene monolayer, we find the σ-bands to be unaffected by the presence of the metal substrate, except for an electrostatic shift that differs substantially between the two layers. For *AB* registry shown in Figure 5, the bottom of the σ-bands near **Γ** is shifted downward by 1.85 and 0.50 eV for the first and second layer, respectively. The magnitude of these shifts is smaller for other interface alignments, varying over 0.5 and 0.3 eV, respectively.

The calculated band dispersions for monolayer graphene on Ru(0001) are essentially identical to those shown in Figure 5a for the inner layer of the graphene bilayer. The bottom of the π-band at Γ is nearly 1 eV lower than pure electrostatic shifts of the σ-bands would suggest. The extent of the π-band shift, which is in good agreement with that found experimentally (Figure 1 b), indicates significant coupling to the Ru d-states. The complete disruption of the linear dispersion of the π-bands near the K point confirms this strong coupling. The d−π coupling results in flat bands near K at energies of −2.5 and −4.5 eV (corresponding to the most intense features in the measured monolayer spectra, Figure 2b), just above E_F and at +2 eV.

As in the experiment (Figure 1d; Figure 3a), the calculated π-bands of the outer layer of bilayer graphene on Ru(0001) (shown in Figure 5a for *AB* registry) closely follow the

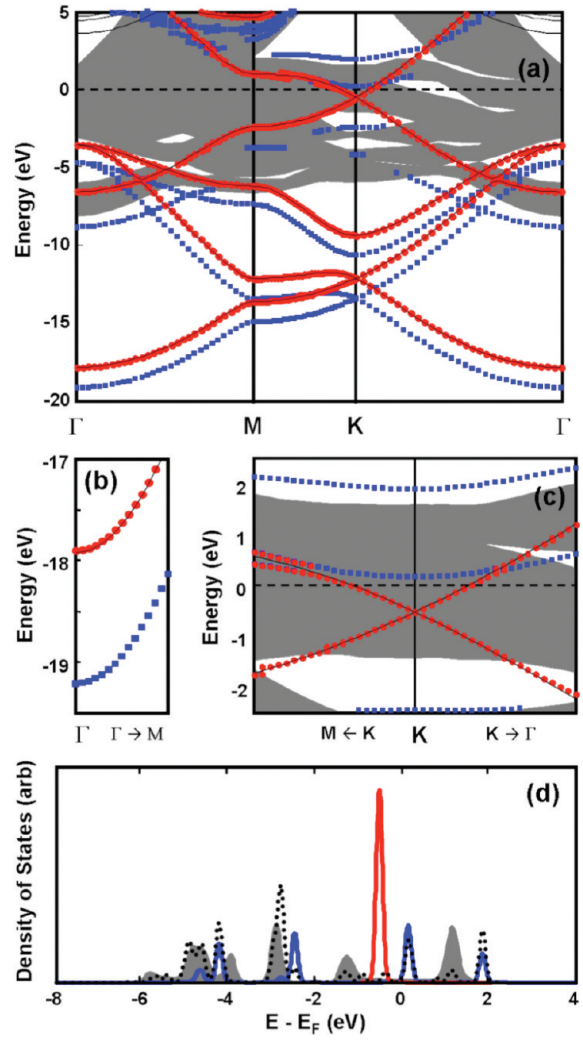

Figure 5. Electronic properties of a commensurate bilayer graphene sample with *AB* alignment to Ru(0001), as shown in Figure 3c. (a) Graphene-dominated bands plotted against the Ru(0001) projected bands in the surface BZ (gray). Square (blue) symbols denote bands with weight projected on the first (inner) graphene layer. Circular (red) symbols denote bands with weight projected on the second (outer) graphene layer. The light black line is the calculated isolated single graphene layer (strained) energy band structure aligned with a downward shift of 0.52 eV relative to the interface Fermi energy. (b) Zoom on the low energy σ-bands near Γ. (c) Zoom on the energy bands near the Fermi level and the K point of the interface BZ. (d) Local density of states at the K point of the interface BZ projected on the interface Ru d-states (dotted), the first (inner) graphene layer (blue), and the second (outer) graphene layer (red) along with the bulk projected Ru(0001) states (gray background). Arbitrary units are used, but each curve is normalized to the correct number of electrons.

expected dispersion for an isolated graphene monolayer. The only effect of the interaction with the underlying Ru and inner graphene layer is a downward shift of the π-band by 0.5 eV, which is in excellent agreement with the measured π-band shift, and modest perturbations upon crossing of the bands of the first layer. The other interfacial registries show the same behavior, but their electrostatic shifts vary over a range of about 0.3 eV. This value provides an estimate for the magnitude of periodic potential modulations acting on the π-bands due to the interfacial moiré structure.

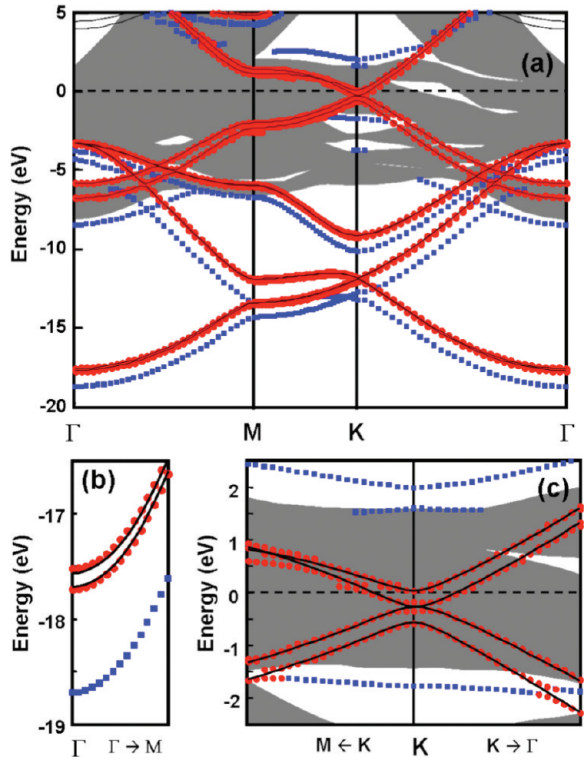

Figure 6. Electronic properties of a commensurate trilayer graphene sample with split alignment to Ru(0001), as shown in Figure 3d. (a) Graphene-dominated bands plotted against the Ru(0001) projected bands in the surface Brillouin zone (gray). Square (blue) symbols denote bands with weight projected on the first (inner) graphene layer. Circular (red) symbols denote bands with weight projected on the second and third (outer) graphene layers. The light black line is the calculated isolated double graphene layer (strained) energy band structure aligned with a downward shift of 0.27 eV relative to the interface Fermi energy. (b) Zoom on the low energy σ bands near Γ. (c) Zoom on the energy bands near the Fermi level and the K point of the interface Brillouin zone.

The calculated band structure (Figure 5c) and local density of states (Figure 5d) near K highlight the different character of the inner and outer layer of the graphene bilayer on Ru(0001), and rationalize the experimentally observed band structure of the bilayer. The strong electronic coupling of the π-states of the inner layer with Ru d-states causes a dramatic reduction of metal- and first-layer graphene derived states, that is, the opening of a gap in these states, around E_F at K. The strongly coupled inner graphene layer hence plays an active role as a buffer, which effectively passivates the metal d-states at the interface. In addition, extended states in the Ru bulk have very low state density at the Fermi level near K. As a result, the π-states of the added outer layer have only minimal interaction with metal and first-layer graphene states and can retain the character of isolated monolayer graphene. In general, a stack of n graphene layers on Ru(0001) has electronic structure close to that of an isolated $(n - 1)$ layer graphene stack, as confirmed by measurements (Figure 3b) and calculations (Figure 6) for trilayer graphene on Ru. This overall evolution of the band structure is strikingly similar to that of epitaxial graphene on SiC,[45] in which the first C-rich layer has a hybrid electronic structure with well-defined σ- but no observable π-bands. Analogous to our observations for graphene on Ru(0001), this buffer layer on SiC can support further sheets that behave essentially like free-standing graphene, except for an electrostatic shift of the Fermi level away from the Dirac point.[36]

Transition metal-supported epitaxial graphene, as considered here, can serve as a convenient model system to study proximity effects between graphene and transition metals. Examples of such effects are the doping of graphene by metal contacts[8,46] and the generation of potential barriers affecting carrier transport,[9] both of which are important for fundamental research on carrier transport phenomena and for graphene-based device technologies. Conventional wisdom would suggest that strongly interacting metals, such as Co, Ni, Pd, and Ru, are ill-suited for exploiting such proximity effects, since their chemical interaction and electronic hybridization with graphene would be too invasive, disrupting the linear π-band dispersion in the Dirac cones. Our results clearly confirm this expectation for monolayer graphene in contact with Ru(0001). However, our study also demonstrates that this strong interaction is strictly confined to the interfacial graphene layer. The chemical interaction is attenuated sufficiently that additional graphene layers couple weakly to the substrate and only experience a shift in electrostatic potential that can be tuned precisely by adjusting the number of graphene layers in the stack.

Acknowledgment. Work performed under the auspices of the U.S. Department of Energy under Contract No. DE-AC02-98CH1-886.

References

(1) Geim, A. K.; Novoselov, K. S. *Nat. Mater.* **2007**, *6* (3), 183.
(2) Novoselov, K. S.; Geim, A. K.; Morozov, S. V.; Jiang, D.; Zhang, Y.; Dubonos, S. V.; Grigorieva, I. V.; Firsov, A. A. *Science* **2004**, *306* (5696), 666.
(3) Berger, C.; Song, Z.; Li, X.; Wu, X.; Brown, N.; Naud, C.; Mayou, D.; Li, T.; Hass, J.; Marchenkov, A. N.; Conrad, E. H.; First, P. N.; de Heer, W. A. *Science* **2006**, *312* (5777), 1191.
(4) Chen, Z.; Lin, Y.-M.; Rooks, M. J.; Avouris, P. *Physica E* **2007**, *40* (2), 228.
(5) Sutter, P. W.; Flege, J.-I.; Sutter, E. A. *Nat. Mater.* **2008**, *7* (5), 406.
(6) Reina, A.; Jia, X.; Ho, J.; Nezich, D.; Son, H.; Bulovic, V.; Dresselhaus, M. S.; Kong, J. *Nano Lett.* **2009**, *9*, 30.
(7) Kim, K. S.; Zhao, Y.; Jang, H.; Lee, S. Y.; Kim, J. M.; Kim, K. S.; Ahn, J.-H.; Kim, P.; Choi, J.-Y.; Hong, B. H. *Nature* **2009**, *457* (7230), 706.
(8) Giovannetti, G.; Khomyakov, P. A.; Brocks, G.; Karpan, V. M.; van den Brink, J.; Kelly, P. J. *Phys. Rev. Lett.* **2008**, *101* (2), 026803.
(9) Lee, E. J. H.; Balasubramanian, K.; Weitz, R. T.; Burghard, M.; Kern, K. *Nat. Nanotechnol.* **2008**, *3* (8), 486.
(10) Pletikosic, I.; Kralj, M.; Pervan, P.; Brako, R.; Coraux, J.; N'Diaye, A. T.; Busse, C.; Michely, T. *Phys. Rev. Lett.* **2009**, *102* (5), 056808.
(11) Brugger, T.; Günther, S.; Wang, B.; Dil, H.; Bocquet, M.-L.; Osterwalder, J.; Wintterlin, J.; Greber, T. *Phys. Rev. B* **2009**, *79*, 045407.
(12) Nagashima, A.; Tejima, N.; Oshima, C. *Phys. Rev. B* **1994**, *50* (23), 17487.
(13) Varykhalov, A.; Sanchez-Barriga, J.; Shikin, A. M.; Biswas, C.; Vescovo, E.; Rybkin, A.; Marchenko, D.; Rader, O. *Phys. Rev. Lett.* **2008**, *101* (15), 157601.
(14) Karpan, V. M.; Giovannetti, G.; Khomyakov, P. A.; Talanana, M.; Starikov, A. A.; Zwierzycki, M.; van den Brink, J.; Brocks, G.; Kelly, P. J. *Phys. Rev. Lett.* **2007**, *99* (17), 176602.
(15) Vazquez de Parga, A. L.; Calleja, F.; Borca, B.; Passeggi Jr, M. C. G.; Hinarejo, J. J.; Guinea, F.; Miranda, R. *Phys. Rev. Lett.* **2008**, *100*, 056807.
(16) Kresse, G.; J, H. *Phys. Rev. B* **1993**, *47*, 558.

(17) Kresse, G.; Hafner, J. *Phys. Rev. B* **1994**, *49*, 14251.
(18) Kresse, G.; Furthmuller, J. *Comput. Mater. Sci.* **1996**, *6*, 15.
(19) Kresse, G.; Furthmuller, J. *Phys. Rev. B* **1996**, *54*, 11169).
(20) Varchon, F.; Feng, R.; Hass, J.; Li, X.; Nguyen, B. N.; Naud, C.; Mallet, P.; Veuillen, J. Y.; Berger, C.; Conrad, E. H.; Magaud, L. *Phys. Rev. Lett.* **2007**, *99* (12), 126805.
(21) Mattausch, A.; Pankratov, O. *Phys. Rev. Lett.* **2007**, *99* (7), 076802.
(22) Vanderbilt, D. *Phys. Rev. B* **1990**, *41*, 7892).
(23) Kresse, G.; Hafner, J. *J. Phys: Condens. Matter* **1994**, *6*, 8245.
(24) Ceperley, D. M.; Alder, B. J. *Phys. Rev. Lett.* **1980**, *45*, 566.
(25) Perdew, J. P.; Zunger, A. *Phys. Rev. B* **1981**, *23*, 5048.
(26) Methfessel, M.; Paxton, A. T. *Phys. Rev. B* **1989**, *40*, 3616.
(27) Blöchl, P. E.; Jepsen, O.; Andersen, O. K. *Phys. Rev. B* **1994**, *49*, 16223.
(28) Pelzer, T.; Ceballos, G.; Zbikowski, F.; Willerding, B.; Wandelt, K.; Thomann, U.; Reuss, C.; Fauster, T.; Braun, J. *J. Phys.: Condens. Matter* **2000**, *12*, 2193.
(29) We used the nearest-neighbor Hamiltonian by Reich et al.[30] with parameters $\varepsilon_{2p} = E_D$ as noted in the text, $\gamma_0 = -3.28$ eV, and overlap $s_0 = 0.03$.
(30) Reich, S.; Maultzsch, J.; Thomsen, C.; Ordejon, P. *Phys. Rev. B* **2002**, *66*, 035412.
(31) Preobrajenski, A. B.; Ng, M. L.; Vinogradov, A. S.; Martensson, N. *Phys. Rev. B* **2008**, *78* (7), 073401.
(32) Oshima, C.; Nagashima, A. *J. Phys: Condens. Matter* **1997**, *9* (1), 1.
(33) Heske, C.; Treusch, R.; Himpsel, F. J.; Kakar, S.; Terminello, L. J.; Weyer, H. J.; Shirley, E. L. *Phys. Rev. B* **1999**, *59* (7), 4680.
(34) Charlier, J. C.; Gonze, X.; Michenaud, J. P. *Phys. Rev. B* **1991**, *43*, 4579.
(35) Ohta, T.; Bostwick, A.; Seyller, T.; Horn, K.; Rotenberg, E. *Science* **2006**, *313* (5789), 951.
(36) Ohta, T.; Bostwick, A.; McChesney, J. L.; Seyller, T.; Horn, K.; Rotenberg, E. *Phys. Rev. Lett.* **2007**, *98* (20), 206802.
(37) Zhou, S. Y.; Gweon, G. H.; Fedorov, A. V.; First, P. N.; de Heer, W. A.; Lee, D. H.; Guinea, F.; Castro Neto, A. H.; Lanzara, A. *Nat. Mater.* **2007**, *6* (10), 770.
(38) Sutter, E. A.; Acharya, D. P.; Sutter, P. W. *Appl. Phys. Lett.* **2009**, *94*, 133101.
(39) Stolyarova, E.; Rim, K. T.; Ryu, S.; Maultzsch, J.; Kim, P.; Brus, L. E.; Heinz, T. F.; Hybertsen, M. S.; Flynn, G. W. *Proc. Natl. Acad. Sci. U.S.A.* **2007**, *104* (22), 9209.
(40) Park, C.-H.; Yang, L.; Son, Y.-W.; Cohen, M. L.; Louie, S. G. *Nat. Phys.* **2008**, *4* (3), 213.
(41) Martoccia, D.; Willmott, P. R.; Brugger, T.; Bjorck, M.; Gunther, S.; Schleputz, C. M.; Cervellino, A.; Pauli, S. A.; Patterson, B. D.; Marchini, S.; Wintterlin, J.; Moritz, W.; Greber, T. *Phys. Rev. Lett.* **2008**, *101* (12), 126102.
(42) We have probed the impact of choosing the LDA by performing generalized gradient approximation calculations with the PBE functional[43] for selected cases. For the split registry, the local bond lengths are essentially the same, but the binding energy is reduced to 0.6 eV, still indicative of significant bond formation. For the BC case, the interaction becomes slightly repulsive and the total energy as a function of Ru-graphene spacing no longer shows a well-defined minimum. This agrees with recent calculations performed with the PBE functional examining a 12 × 12 graphene layer on an 11 × 11 Ru(0001) slab supercell.[44] While LDA-based calculations overestimate binding for weakly interacting layered systems (graphite *c*-axis lattice parameter too small), PBE-based calculations generally give no binding for such systems (graphitic layers are not bound). Thus, interface interaction suggests that the graphene regions near BC registry in the moiré may be somewhat further (say 0.1 Å) from the Ru surface than our LDA calculations indicate (2.20 Å), although lateral strain interactions may enhance the buckling.
(43) Perdew, J. P.; Burke, K.; Ernzerhof, M. *Phys. Rev. Lett.* **1996**, *77*, 3865.
(44) Wang, B.; Bocquet, M.-L.; Marchini, S.; Günther, S.; Wintterlin, J. *Phys. Chem. Chem. Phys.* **2008**, *10*, 3530.
(45) Emtsev, K. V.; Speck, F.; Seyller, T.; Ley, L.; Riley, J. D. *Phys. Rev. B* **2008**, *77*, 155303.
(46) Uchoa, B.; Lin, C.-Y.; Castro Neto, A. H. *Phys. Rev. B* **2008**, *77*, 035420.

NL901040V